4-7-2021

Physics-guided Neural Network for Predicting Chemical Signatures

Cara Murphy
Systems & Technology Research

John Kerekes
Rochester Institute of Technology

Recommended Citation
Cara P. Murphy and John P. Kerekes, "Physics-guided neural network for predicting chemical signatures," Appl. Opt. 60, 3176-3181 (2021) https://doi.org/10.1364/AO.420688

Physics-guided Neural Network for Predicting Chemical Signatures

CARA P. MURPHY[1,2,*] AND JOHN KEREKES[2]

[1] *Systems & Technology Research, 600 West Cummings Park, Woburn, MA 01801, USA*
[2] *Chester F. Carlson Center for Imaging Science, Rochester Institute of Technology, 54 Lomb Memorial Drive, Rochester, NY 14623, USA*
[*] *Cara.Murphy@STResearch.com*

Abstract: Achieving high classification accuracy on trace chemical residues in active spectroscopic sensing is challenging due to the limited amount of training data available to the classifier. Such classifiers often rely on physics-based models for generating training data though these models are not always accurate when compared to measured data. To overcome this challenge, we developed a physics-guided neural network (PGNN) for predicting chemical reflectance for a set of parameterized inputs that is more accurate than the state-of-the-art physics-based signature model for chemical residues. After training the PGNN, we use it to generate a library of predicted spectra for training a classifier. We compare the classification accuracy when using this PGNN library versus a library generated by the physics-based model. Using the PGNN, the average classification accuracy increases from 0.623 to 0.813 on real chemical reflectance data, including data from chemicals not included in the PGNN training set.

1. Introduction

Identifying trace amounts of chemicals on surfaces is a desirable capability for a wide range of defense, intelligence, and law enforcement applications [1]. Chemicals of interest for these applications include explosives, chemical warfare agents, narcotics, etc. Active infrared (IR) spectroscopy is arguably the only technique capable of achieving high-sensitivity standoff identification of trace chemicals on surfaces while achieving high areal coverage rates [2–4]. A notional example of an active long-wave IR (LWIR) hyperspectral imaging (HSI) system is shown in Figure 1. The system operates by measuring the spectral reflectance, or the portion of which is reflected back towards the sensor, of the target surface in the LWIR portion of the optical spectrum using quantum cascade lasers (QCL) as the illumination source [3, 5, 6] and comparing the measured signature to a spectral library of reference signatures. Because of the wide range of relevant applications for this type of technology, the spectral library often includes hundreds to thousands of reference chemicals, making the association of measured data with the reference data very challenging.

Such a system might use one of several classes of chemical classification algorithms, including subspace methods, least squares approaches, machine or deep learning, etc. [8, 9] to associate a measurement with a reference chemical signature. Machine and deep learning algorithms, in particular, have the benefit of being able to learn arbitrary rules to distinguish between data [10]. Over the last two decades, neural networks (NN), or artificial neural networks (ANN), have become known as powerful machine learning tools for solving a variety of problems. More recent research efforts use 1D convolutional neural networks (CNNs) for classifying pixels in hyperspectral imagery [11]. For example, Riese and Keller developed the LucasCNN for classifying soil in the Land Use / Cover Area Frame Statistical Survey (LUCAS) hyperspectral dataset [12].

The major disadvantage in using any machine learning method for classification is that they require a large amount of training data [13]. Therefore, it is common in many applications to

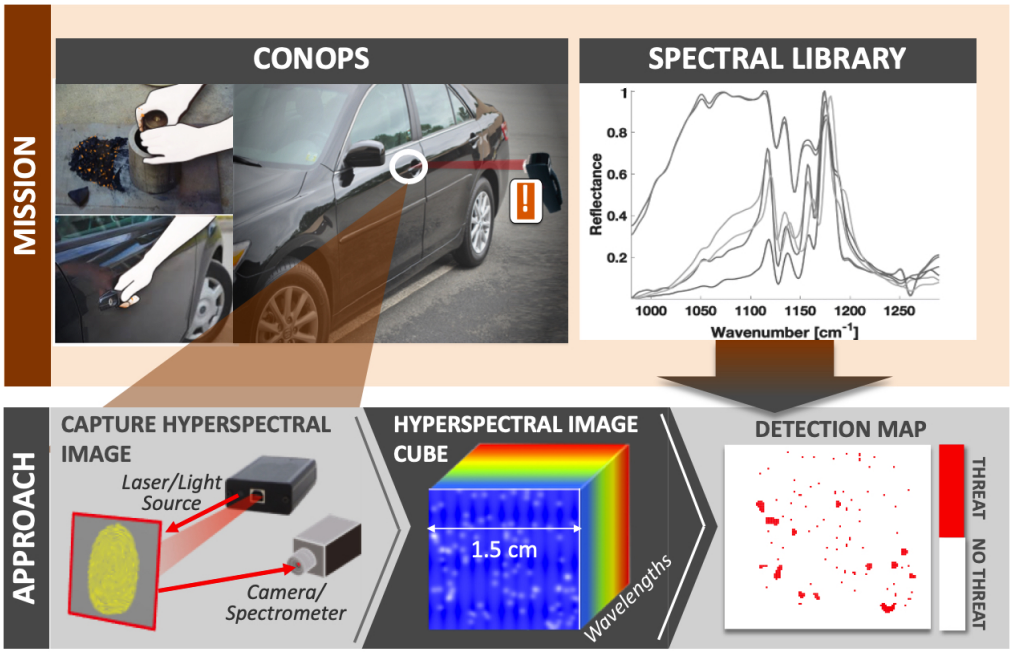

Fig. 1. A notional depiction of standoff trace chemical classification via an active spectroscopic instrument. The reference signature library is pertinent to the system's ability to identify chemicals of interest [7].

train a classifier using simulated data [14]. Active spectroscopy of trace chemicals is one of those applications because it is time-consuming and inefficient to measure all combinations of chemicals, chemical form, and substrate. However, developing a signature simulation model for trace chemical classification applications is challenging due to the phenomenological complexities [15–28]. This is problematic because the performance of machine learning classifiers degrades when the training data domain differs from the test data domain [29]. Domain adaptation has recently demonstrated significant utility in translating data between domains (e.g. from the simulated data domain to the measured data domain) [30–36]. Specifically, a 1D conditional generative adversarial network (GAN) has been shown to improve classification accuracy on active spectroscopic reflectance signatures of chemicals on surfaces by translating a simulated training library to the measured data domain [37]. The classification accuracy improvement in [37], however, is limited on chemicals that are not included in the GAN training set.

In recent years, the fusion of task-driven data science models with theoretical principles of physics has produced models that are more accurate than those which derive solely from physics [38–40]. For example, the physics-guided neural network (PGNN) defined in [41] achieves an average reduction in model error of 46% relative to physical models when predicting lake temperatures. The research in this paper applies the PGNN model concepts for predicting chemical reflectance signatures for training a chemical classifier. The end goal of this research is to present a method for producing a library of more realistic spectral signatures capable of achieving high classification accuracy, as compared to libraries generated from state-of-the-art physics-based methods, in real active spectroscopic data.

This paper is structured as follows. Section 2.1 explains the state-of-the-art physics-based model for predicting trace chemical reflectance signatures. Section 2.2 describes the PGNN approach for generating more accurate chemical reflectance signatures for comparing to the physics-based

approach. Next, Section 2.3 discusses the recent LucasCNN classifier for hyperspectral data and how it is used in this research to demonstrate the improvement made by the PGNN. The available measured data used for analysis are described in Section 2.4 and Section 2.5 explains the data preparation and model testing and training steps for performing analysis. The Results section (Section 3) shows a comparison of chemical classification accuracy with and without the PGNN when classifying measured chemical signatures as well as a qualitative comparison between the physics-based model outputs and the PGNN model outputs.

2. Materials and Methods

2.1. Physics-Based Signature Model for Chemicals on Surfaces

This work considers reflectance signatures of trace chemical residues. The physics-based model used for predicting trace chemical residue reflectance signatures in this research is the sparse transfer matrix (STM) model [7]. STM is designed to specifically handle the physics of trace chemical residue. STM assumes a thin chemical film with sparse coverage in the contaminated area. The regions containing chemical are assumed to have a non-uniform thickness that follows a log-normal distribution:

$$R_{STM}(\lambda) = FF\ R_{chem}(\lambda) + (1 - FF)\ SSF\ R_{sub}(\lambda), \tag{1}$$

where λ is the wavenumber, FF is the fill factor (the fraction of a pixel covered by the chemical), SSF is the substrate scale factor (i.e. a proxy for the bidirectional reflectance factor), R_{sub} is the measured bare substrate reflectance term, and R_{chem} is the chemical reflectance term calculated by the transfer matrix (TM) model [42,43]. The TM model uses the Fresnel reflection coefficients at the air / chemical (r_1) and chemical / substrate interface (r_1) to calculate reflectance [44–47]:

$$r_1(\lambda) = \frac{\tilde{n}^*_{air} - \tilde{n}^*_{chem}}{\tilde{n}^*_{air} + \tilde{n}^*_{chem}} \tag{2}$$

and

$$r_2(\lambda) = \frac{\tilde{n}^*_{chem} - \tilde{n}^*_{sub}}{\tilde{n}^*_{chem} + \tilde{n}^*_{sub}}, \tag{3}$$

where * indicates the complex conjugate. The fill factor is a function of the chemical density, mean particle diameter, particle size standard deviation, and the chemical concentration [7].

2.2. Physics-Guided Neural Network for Chemicals on Surfaces

The PGNN developed by Karpatne et al. is a hybrid physics-based data science model initially developed for modeling lake water temperatures. The authors of the PGNN model describe a standard NN model as $f_{NN} : D \rightarrow Y$, where D is the set of input parameters and Y is the target variable. Similarly, a pure physics-based model can be expressed as $f_{PHY} : D \rightarrow Y$. The PGNN model, however, is expressed as $f_{PGNN} : [D,\ Y_{PHY}] \rightarrow Y$, where the inputs include all the relevant parameters as well as the output of the physics-based simulator, Y_{PHY} (Karpatne et al. use the state-of-the-art physics-based General Lake Model [48]).

We use the general PGNN model design [49] for predicting chemical reflectance signatures on surfaces. The model is scaled up to 16 hidden layers and 64 nodes per layer to handle to complexity of the trace chemical reflectance signatures. The model input parameters, D, are shown in Table 1. The substrate ID is an integer assigned to each substrate in the study. We provide the model with the substrate ID as there are substrate attributes beyond substrate reflectance and optical constants that can affect the reflectance of a chemical on the surface (e.g. surface roughness, dielectric properties, specularity, etc.). Providing the substrate ID enables the model to learn some of these substrate effects from the measured reflectance. We use the STM

simulation output as the input for Y_{PHY} and the corresponding measured reflectance as the target variable, Y. The PGNN model was found to have the best performance when it was also supplied the preliminary terms r_1, r_2, and R_{chem} calculated by the STM model. We express our full model as $f_{PGNN_{chem}} : [D,\ Y_{terms},\ Y_{PHY}] \rightarrow Y$, where Y_{terms} is comprised of the preliminary terms of the STM model. All optical constant and reflectance inputs (including r_1 and r_2) are normalized to be between 0 and 1 for training the PGNN. We use the root-mean-square error as the loss function as in [41] and [49].

Table 1. The PGNN input parameters for predicting chemical reflectance.

	Parameter
1	Wavenumber, λ $[m^{-1}]$
2	Substrate ID
3	Chemical Concentration $[mg/cm^2]$
4	Mean Particle Diameter, μ $[\mu m]$
5	Particle Size Standard Deviation, σ $[\mu m]$
6	Substrate Scale Factor, SSF
7	Chemical Density $[mg/cm^3]$
8	Substrate Complex Optical Constant, $\tilde{n}_{sub}$
9	Substrate Reflectance, R_{sub}
10	Chemical Complex Optical Constant, $\tilde{n}_{chem}$

2.3. Chemical Classification

The main goal of this work is to improve chemical classification performance using PGNN-predicted spectra. In particular, we are interested in the performance improvement when classifying chemicals that were not used to train the PGNN. To demonstrate this, we compare classification accuracy on several chemicals when training on STM-predicted spectra versus PGNN-predicted spectra. We use the LucasCNN model as the classification algorithm for these experiments. For each experiment, the LucasCNN model is trained for 10 epochs using a batch size of 128 and the the Adam optimizer [50]. We provide details on the training and test data in the next sections.

2.4. Chemical Reflectance Data

The chemical samples used in this research were provided by Johns Hopkins University Applied Physical Laboratory (JHU/APL). JHU/APL prepared various substrate samples with chemical residue contamination at a range of concentrations. Trace chemical residue is defined as the film-like residue that remains on a surface after the evaporation of a solvent that contained the chemical. The solid chemicals were first dissolved in a solvent and then evenly airbrushed over the substrates using a mechanical arm. The active LWIR hyperspectral reflectance measurements were collected by the system developed by Block MEMS for the IARPA SILMARILS (Standoff ILluminator for Measuring Absorbance and Reflectance Infrared Light Signatures) program [5, 6, 51]. In total, JHU/APL prepared six different chemicals on four different substrates at concentrations ranging

from 50 to 150 $\mu g/cm^2$, though not all of the chemicals were used on all of the substrates. The breakdown of measured samples per chemical, substrate, and concentration are shown in Table 2.

The measured data is required for training the PGNN (i.e. it is used as the target variable, Y) as well as testing the classifier accuracy. Of particular interest to this research is the improvement in classification accuracy on chemicals that are not used for training the PGNN. In other words, can the PGNN improve performance on chemicals we have never measured before? Therefore, we separate the measured data into two datasets: dataset 1 (DS1) is used for training the PGNN as well as testing the classifier and dataset 2 (DS2) is used for testing the classifier only. To ensure the PGNN is as robust as possible to the substrate, we include all measurements of aspirin, pentaerythritol, and saccharin (i.e. the three chemicals measured on all four substrates) in DS1. All measurements of caffeine, lactose, and naproxen comprise DS2.

Table 2. The number of measured samples and their concentrations for each unique chemical / substrate combination used in this study.

Substrate / Chemical	Cardboard	Glass	High-density Polyethylene (HDPE)	Rough Aluminum
Aspirin	14 at 50 $\mu g/cm^2$	1 at 100 $\mu g/cm^2$	2 at 100 $\mu g/cm^2$	7 at 100 $\mu g/cm^2$
Caffeine	15 at 50 $\mu g/cm^2$	1 at 50 $\mu g/cm^2$ 6 at 100 $\mu g/cm^2$ 3 at 150 $\mu g/cm^2$		3 at 100 $\mu g/cm^2$
Lactose		1 at 50 $\mu g/cm^2$ 3 at 100 $\mu g/cm^2$		3 at 50 $\mu g/cm^2$
Naproxen		1 at 100 $\mu g/cm^2$ 2 at 150 $\mu g/cm^2$		1 at 100 $\mu g/cm^2$ 3 at 150 $\mu g/cm^2$
Penta-erythritol	15 at 50 $\mu g/cm^2$	2 at 150 $\mu g/cm^2$	3 at 100 $\mu g/cm^2$	5 at 100 $\mu g/cm^2$ 1 at 150 $\mu g/cm^2$
Saccharin	2 at 50 $\mu g/cm^2$ 3 at 100 $\mu g/cm^2$	6 at 100 $\mu g/cm^2$	2 at 100 $\mu g/cm^2$	5 at 100 $\mu g/cm^2$ 1 at 150 $\mu g/cm^2$

We generate the simulated data for training the PGNN and classifier using the STM model described in Section 2.1. The STM model has three parameters the user must set [7]: the particle diameter mean and standard deviation and the substrate scale factor. The range of parameter values used in this study are summarized in Table 3. (Information for setting these parameter values can be found in [7].) To create the STM-predicted library, we generate an STM simulation for each parameter combination in Table 3 for each chemical, substrate, and concentration (i.e. 125 parameter combinations for 6 chemicals, 4 substrates, and 3 concentrations). This library is used for training the LucasCNN classifier later. The output of the STM simulator is the R_{STM} term. To train the PGNN, each measurement Y in DS1 needs a corresponding R_{STM} term as well as the corresponding set of parameters in Table 1. For each measurement in DS1, we select the entry in the STM library that provides the best fit (in an ℓ^2 sense) to the measurement to generate the PGNN inputs, $[D,\ Y_{terms},\ Y_{PHY}]$, where the values of D are the parameters used to find

the best fitting R_{STM} and Y_{terms} are the preliminary terms used to calculate R_{STM}. Both the simulated and real data used for this analysis consist of 200 wavenumbers from 980 to 1290 cm^{-1} with an 1.55 cm^{-1} spacing and are normalized prior to training the PGNN or LucasCNN models.

Table 3. STM tunable parameters and their values used for our experiments.

Parameter	Experiment Values
Mean particle diameter, μ	0.10, 0.32, 1.00, 3.20, 10.00 μm
Particle diameter standard deviation, σ	0.10, 0.20, 0.40, 0.79, 1.59 μm
Substrate scale factor, SSF	0.10, 0.32, 1.00, 3.20, 10.00

2.5. Data Augmentation and Model Training and Testing

Neither DS1 nor DS2 contain sufficient samples for training or testing. To augment the datasets for training and testing, we replicate each measurement for a total of 100 entries per pair and add white Gaussian noise to each. (The sensor used for data collection was shot-noise limited with noise following an approximately Gaussian distribution.) Additionally, we add a random gradual slope in magnitude of up to ±20% of the total magnitude and a random wavenumber shift between $\pm 4.65 cm^{-1}$ to the PGNN training data. In addition to increasing the number of unique samples for training, the data augmentation steps also increase the PGNN model's robustness to common calibration errors in active spectroscopic data. The random slope adds robustness to slight reflectance calibration offsets (as seen in measurements of bare rough aluminum during the data collection) while the wavenumber shift adds robustness to calibration errors in the QCLs (i.e. wavenumber drift [52]).

The PGNN model is trained using a subset of the augmented DS1 data and corresponding input parameters. To obtain training and testing data, DS1 is split across unique measurements (i.e. all 100 entries derived from a particular measurement exist entirely in either the training or test set) with stratification across the chemical label. We use a training ratio of 0.8 such that we have 5500 spectra for training and 1400 for testing in DS1. When training the model, we use a validation ratio of 0.1. The model is trained for 5 epochs using a batch size of 200 and the Adagrad optimizer [53]. Each training epoch takes ~2 minutes on a 2019 MacBook Pro running macOS 10.15.7 with a 2.4 GHz 8-Core Intel Core i9 processor.

After the PGNN is trained, we compare classification accuracy using the STM-predicted library described in Section 2.4 and the PGNN-predicted library for training the LucasCNN model. The PGNN-predicted library is the output of the trained PGNN model given the STM library and corresponding parameters as inputs. Generating the PGNN-predicted library takes ~1.7 minutes (<0.02 seconds per spectrum) on the same machine used for training. A separate LucasCNN model instance is trained for each library. Both model instances are tested on the same measured data from the DS1 test set (1400 spectra) and DS2 (4200 spectra). Due to the unequal number of samples per class in DS1, we perform a 10-fold training/test data split and average classification accuracy results across the 10 experiments, retraining the PGNN and LucasCNN models each time. The classification performance on DS1 chemicals tells us how well the PGNN learns to predict signatures for the chemicals included in the PGNN training. The classification performance on DS2 chemicals tells us how well the PGNN will predict signatures for chemicals we have never measured before.

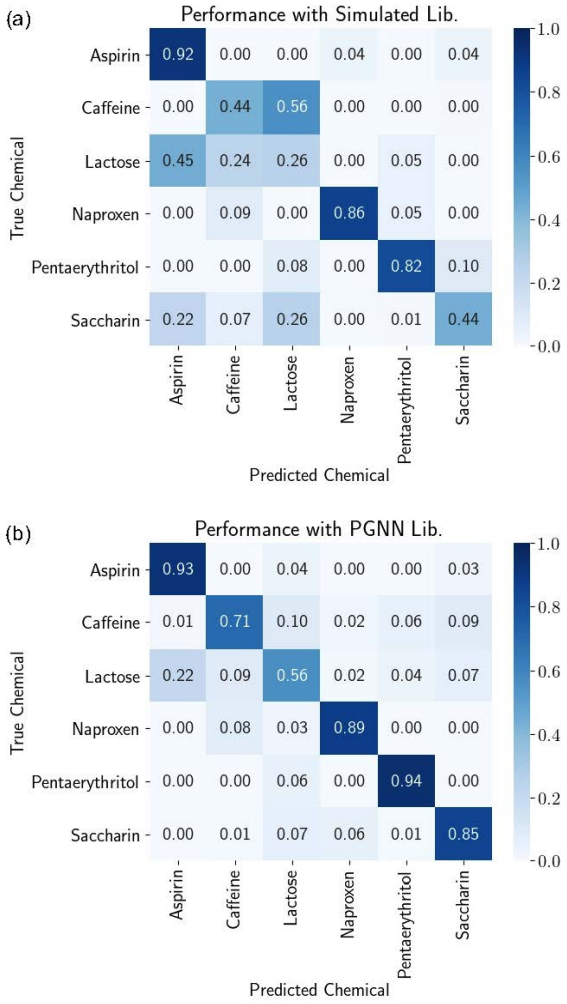

Fig. 2. Normalized confusion matrices for each LucasCNN model training method when testing on the measured test data. Training the LucasCNN model on the STM-predicted library (a) gives an overall classification accuracy of 0.623 across all chemicals while training on the PGNN-predicted library (b) gives an overall accuracy of 0.813. Notably, the PGNN library doubled the classification accuracy on lactose, one of the chemicals that were excluded from the PGNN training set.

3. Results and Discussion

After training each 10-fold iteration of the PGNN model, we perform classification on the measured test data using the LucasCNN model when training with the STM versus PGNN outputs. We compute the overall classification accuracy (i.e. we sum the number of chemicals identified as belonging to a particular class across all iterations and divide by the total number of test measurements per class). The ratios of correct and incorrect chemical predictions are shown in Figure 2 for each classifier training method. The classifier achieves better performance on all chemicals using the PGNN library. Overall, the PGNN library increases the classification accuracy from 0.623 to 0.813 with significant improvement on some of the more challenging chemicals that were excluded from the PGNN training set: caffeine and lactose.

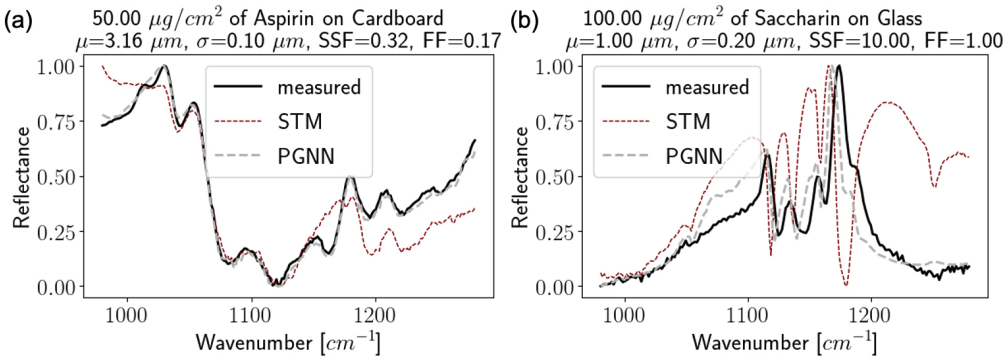

Fig. 3. Measured spectra of (a) 50 $\mu g/cm^2$ of aspirin on cardboard and (b) 100 $\mu g/cm^2$ of saccharin on glass are shown by the black curves. The corresponding STM predictions are shown by the dotted red curves while the PGNN predictions are shown by the dashed gray curves. Overall, the PGNN predictions provide a better match to the measured data.

A more qualitative result is shown in Figure 3. Measured spectra of aspirin on cardboard and saccharin on glass are shown on the same plot as their corresponding best-fitting STM simulations and their corresponding PGNN-predicted spectra from a single trained PGNN model. As shown in Figure 3, even the best fits from the STM simulation model do not provide a perfect fit to the measured data. The PGNN spectra, however, provide a very strong fit to the measured data. Note, the measured spectra shown in these results were taken from the DS1 test set rather than the PGNN training set.

4. Summary

In this work, we present a novel concept for enhancing trace chemical reflectance signature predictions. We begin with the physics-based STM signature model for simulating chemical residue reflectance. We suggest that though the model is best-suited for modeling chemical residue phenomenology, there are some limitations in its ability to fit to real data. To solve this problem, we trained a PGNN to more accurately predict chemical reflectance based on parameterized inputs. We demonstrate the performance of the PGNN by comparing classification accuracy when a classifier is trained using the STM library versus the PGNN library. Overall, the PGNN library increases the classification accuracy from 0.623 to 0.813 and much of the improvement is demonstrated on chemicals that were not included in the PGNN training set. These results indicate that the PGNN model is robust to new chemicals (and possibly new substrates, parameters, etc.) and can be used to improve chemical classification performance on all targets, including those that have not been measured previously. As stated in Section 2.5, the number of samples used for this analysis is limited. The number of unique combinations of physical parameters we can use for training the PGNN model is also limited by the availability of representative data. We expect the PGNN to better generalize the mapping from the input parameter space to the measured reflectance space with more variable training data. Therefore, we also expect the classification performance improvement to increase as more data becomes available.

Acknowledgments

The authors thank Dr. Kristin DeWitt, IARPA program manager of the SILMARILS program for her support as well as the SILMARILS test and evaluation team for providing contaminated

samples used for analysis and corresponding metadata. Additionally, the authors thank their colleagues from Systems & Technology Research and Block MEMS for their provided insights.

Disclosures

The authors declare no conflicts of interest.

References

1. K. DeWitt, "Advances in active infrared spectroscopy for trace chemical detection ," in *Algorithms, Technologies, and Applications for Multispectral and Hyperspectral Imagery XXV,* vol. 10986 M. Velez-Reyes and D. W. Messinger, eds., International Society for Optics and Photonics (SPIE, 2019), pp. 151 – 162.
2. M. C. Phillips and B. E. Bernacki, "Infrared spectroscopy of explosives residues: Measurement techniques and spectral analysis," in *Laser-based optical detection of explosives,* P. M. Pellegrino, E. L. Holthoff, and M. E. Farrell, eds. (CRC Press, 2015), pp. 213–256.
3. P. Kotidis, E. R. Deutsch, and A. Goyal, "Standoff detection of chemical and biological threats using miniature widely tunable QCLs," in *Micro- and Nanotechnology Sensors, Systems, and Applications VII,* vol. 9467 T. George, A. K. Dutta, and M. S. Islam, eds., International Society for Optics and Photonics (SPIE, 2015).
4. A. K. Goyal and T. R. Myers, "Active mid-infrared reflectometry and hyperspectral imaging," in *Laser-Based Optical Detection of Explosives,* P. M. Pellegrino, E. L. Holthoff, and M. E. Farrell, eds. (CRC Press, 2015).
5. D. B. Kelley, A. K. Goyal, N. Zhu, D. A. Wood, T. R. Myers, P. Kotidis, C. Murphy, C. Georgan, G. Raz, R. Maulini, and A. Müller, "High-speed mid-infrared hyperspectral imaging using quantum cascade lasers," in *Chemical, Biological, Radiological, Nuclear, and Explosives (CBRNE) Sensing XVIII,* vol. 10183 A. W. F. III and J. A. Guicheteau, eds., International Society for Optics and Photonics (SPIE, 2017), pp. 19 – 28.
6. D. B. Kelley, D. Wood, A. K. Goyal, and P. Kotidis, "High-speed and large-area scanning of surfaces for trace chemicals using wavelength-tunable quantum cascade lasers," in *Chemical, Biological, Radiological, Nuclear, and Explosives (CBRNE) Sensing XIX,* vol. 10629 J. A. Guicheteau, A. W. F. III, and C. R. Howle, eds., International Society for Optics and Photonics (SPIE, 2018), pp. 31 – 37.
7. C. P. Murphy, J. P. Kerekes, D. A. Wood, and A. K. Goyal, "Practical model for improved classification of trace chemical residues on surfaces in active spectroscopic measurements," Opt. Eng. **59**, 1 – 13 (2020).
8. G. Raz, C. Murphy, C. Georgan, R. Greenwood, R. K. Prasanth, T. Myers, A. Goyal, D. Kelley, D. Wood, and P. Kotidis, "Novel trace chemical detection algorithms: a comparative study," in *Algorithms and Technologies for Multispectral, Hyperspectral, and Ultraspectral Imagery XXIII,* vol. 10198 M. Velez-Reyes and D. W. Messinger, eds. (2017), p. 101980D.
9. M. Eismann, *Hyperspectral Remote Sensing*, Press Monographs (SPIE, 2012).
10. M. G. Madden and T. Howley, "A machine learning application for classification of chemical spectra," in *Applications and Innovations in Intelligent Systems XVI,* T. Allen, R. Ellis, and M. Petridis, eds. (Springer London, London, 2009), pp. 77–90.
11. W. Hu, Y. Huang, L. Wei, F. Zhang, and H. Li, "Deep convolutional neural networks for hyperspectral image classification," J. Sensors **2015**, 258619 (2015).
12. F. M. Riese and S. Keller, "Soil texture classification with 1d convolutional neural networks based on hyperspectral data," ISPRS Annals Photogramm. Remote. Sens. Spatial Inf. Sci. **IV-2/W5**, 615–621 (2019).
13. I. Goodfellow, Y. Bengio, and A. Courville, *Deep Learning* (MIT Press, 2016). http://www.deeplearningbook.org.
14. N. Ødegaard, A. O. Knapskog, C. Cochin, and J. Louvigne, "Classification of ships using real and simulated data in a convolutional neural network," in *2016 IEEE Radar Conference (RadarConf),* (2016), pp. 1–6.
15. K. DeWitt, "Machine learning for better trace chemical detection ," in *Algorithms, Technologies, and Applications for Multispectral and Hyperspectral Imagery XXV,* vol. 10986 M. Velez-Reyes and D. W. Messinger, eds., International Society for Optics and Photonics (SPIE, 2019), pp. 376 – 385.
16. M. Phillips, J. Suter, B. Bernacki, and T. Johnson, "Challenges of infrared reflective spectroscopy of solid-phase explosives and chemicals on surfaces," Proc. SPIE - The Int. Soc. for Opt. Eng. **8358**, 23– (2012).
17. J. Suter, B. Bernacki, and M. Phillips, "Spectral and angular dependence of mid-infrared diffuse scattering from explosives residues for standoff detection using external cavity quantum cascade lasers," Appl. Phys. B **108** (2012).
18. M. L. Wenrich and P. R. Christensen, "Optical constants of minerals derived from emission spectroscopy: Application to quartz," J. Geophys. Res. Solid Earth **101**, 15921–15931 (1996).
19. P. D. Kleiber, V. H. Grassian, M. A. Young, and P. K. Hudson, "T-matrix studies of aerosol particle shape effects on ir resonance spectral line profiles and comparison with an experiment," J. Geophys. Res. Atmospheres **114** (2009).
20. V. P. Tishkovets, E. V. Petrova, and M. I. Mishchenko, "Scattering of electromagnetic waves by ensembles of particles and discrete random media," J. Quant. Spectrosc. Radiat. Transf. **112**, 2095 – 2127 (2011). Polarimetric Detection, Characterization, and Remote Sensing.
21. B. H. Horgan, E. A. Cloutis, P. Mann, and J. F. Bell, "Near-infrared spectra of ferrous mineral mixtures and methods for their identification in planetary surface spectra," Icarus **234**, 132 – 154 (2014).

22. L. Moroz, A. Basilevsky, T. Hiroi, S. Rout, D. Baither, C. van der Bogert, O. Yakovlev, A. Fisenko, L. Semjonova, V. Rusakov, D. Khramov, N. Zinovieva, G. Arnold, and C. Pieters, "Spectral properties of simulated impact glasses produced from Martian soil analogue JSC Mars-1," Icarus **202**, 336 – 353 (2009).
23. L. Kirkland, K. Herr, and P. Adams, "Infrared stealth surfaces: Why TES and THEMIS may miss some substantial, mineral deposits on Mars and implications for remote sensing of planetary surfaces," J. Geophys. Res. **108** (2003).
24. B. Hapke, *Theory of Reflectance and Emittance Spectroscopy* (Cambridge University Press, 2012), 2nd ed.
25. R. Hudson, P. Gerakines, and M. Moore, "Infrared spectra and optical constants of astronomical ices: II. ethane and ethylene," Icarus **243**, 148 – 157 (2014).
26. A. Politano, G. Chiarello, G. Benedek, E. Chulkov, and P. Echenique, "Vibrational spectroscopy and theory of alkali metal adsorption and co-adsorption on single-crystal surfaces," Surf. Sci. Reports **68**, 305 – 389 (2013).
27. M. Van Thiel, E. D. Becker, and G. C. Pimentel, "Infrared studies of hydrogen bonding of water by the matrix isolation technique," The J. Chem. Phys. **27**, 486–490 (1957).
28. K. Buijs and G. R. Choppin, "Near-infrared studies of the structure of water. I. pure water," The J. Chem. Phys. **39**, 2035–2041 (1963).
29. H. Shimodaira, "Improving predictive inference under covariate shift by weighting the log-likelihood function," J. Stat. Plan. Inference **90**, 227 – 244 (2000).
30. M. Wang and W. Deng, "Deep visual domain adaptation: A survey," Neurocomputing **312**, 135 – 153 (2018).
31. L. Bruzzone and M. Marconcini, "Domain adaptation problems: A DASVM classification technique and a circular validation strategy," IEEE Transactions on Pattern Analysis Mach. Intell. **32**, 770–787 (2010).
32. W. Chu, F. De la Torre, and J. F. Cohn, "Selective transfer machine for personalized facial expression analysis," IEEE Transactions on Pattern Analysis Mach. Intell. **39**, 529–545 (2017).
33. M. Gheisari and M. S. Baghshah, "Unsupervised domain adaptation via representation learning and adaptive classifier learning," Neurocomputing **165**, 300 – 311 (2015).
34. B. Gong, K. Grauman, and F. Sha, "Connecting the dots with landmarks: Discriminatively learning domain-invariant features for unsupervised domain adaptation," in *Proceedings of the 30th International Conference on Machine Learning,* vol. 28 of *Proceedings of Machine Learning Research* S. Dasgupta and D. McAllester, eds. (PMLR, Atlanta, Georgia, USA, 2013), pp. 222–230.
35. S. Pachori, A. Deshpande, and S. Raman, "Hashing in the zero shot framework with domain adaptation," Neurocomputing **275**, 2137 – 2149 (2018).
36. S. J. Pan, I. W. Tsang, J. T. Kwok, and Q. Yang, "Domain adaptation via transfer component analysis," IEEE Transactions on Neural Networks **22**, 199–210 (2011).
37. C. P. Murphy and J. Kerekes, "1D conditional GAN for spectrum-to-spectrum translation of simulated chemical reflectance signatures," J. Spectr. Imaging (2021). [Submitted and under review.].
38. A. Karpatne, G. Atluri, J. H. Faghmous, M. Steinbach, A. Banerjee, A. Ganguly, S. Shekhar, N. Samatova, and V. Kumar, "Theory-guided data science: A new paradigm for scientific discovery from data," IEEE Transactions on Knowl. Data Eng. **29**, 2318–2331 (2017).
39. T. Sejnowski, P. Churchland, and J. Movshon, "Putting big data to good use in neuroscience," Nat. neuroscience **17**, 1440–1 (2014).
40. L. Bruzzone, "The role of physical models in the artificial intelligence era," in *Proceedings of the 2020 IEEE International Geoscience and Remote Sensing Symposium (IGARSS),* (2020).
41. A. Karpatne, W. Watkins, J. S. Read, and V. Kumar, "Physics-guided neural networks (PGNN): an application in lake temperature modeling," ArXiv **abs/1710.11431** (2017).
42. T. Myers, D. Wood, A. K. Goyal, D. Kelley, P. Kotidis, G. Raz, C. Murphy, and C. Georgan, "Mid-infrared hyperspectral simulator for laser-based detection of trace chemicals on surfaces," in *Algorithms and Technologies for Multispectral, Hyperspectral, and Ultraspectral Imagery XXIII,* vol. 10198 M. Velez-Reyes and D. W. Messinger, eds., International Society for Optics and Photonics (SPIE, 2017), pp. 123 – 132.
43. C. C. Katsidis and D. I. Siapkas, "General transfer-matrix method for optical multilayer systems with coherent, partially coherent, and incoherent interference," Appl. Opt. **41**, 3978–3987 (2002).
44. O. S. Heavens, "Optical properties of thin films," Reports on Prog. Phys. **23**, 1–65 (1960).
45. X. Tian, C. Zhuang-Qi, and F. Jing-Huai, "The analytical transfer matrix method for quantum reflection," Chin. Phys. B **19**, 040307 (2010).
46. L. Landau and E. Lifshitz, *Quantum Mechanics: Non-Relativistic Theory* (Elsevier Ltd., 1977), 3rd ed.
47. L. Landau and E. Lifshitz, *Electrodynamics of Continuous Media* (Butterworth-Heinemann, 1984black), 2nd ed.
48. M. Hipsey, L. Bruce, , and D. Hamilton, *GLM - General Lake Model: Model overview and user information*, The University of Western Australia, Perth, Australia.
49. A. Daw, "PGNN," https://github.com/arkadaw9/PGNN (2019). [Online; last commit 18-November-2019].
50. D. P. Kingma and J. Ba, "Adam: A method for stochastic optimization," (2017).
51. D. Wood, D. B. Kelley, A. K. Goyal, and P. Kotidis, "Mid-infrared reflection signatures for trace chemicals on surfaces," in *Chemical, Biological, Radiological, Nuclear, and Explosives (CBRNE) Sensing XIX,* vol. 10629 J. A. Guicheteau, A. W. F. III, and C. R. Howle, eds., International Society for Optics and Photonics (SPIE, 2018), pp. 128 – 133.
52. C. Dyroff, *Tunable Diode Laser Absorption Spectroscopy for Trace Gas Measurements with High Sensitivity and Low Drift*, Karlsruhe series in photonics & communications (KIT Scientific Publishing, 2009).

53. J. Duchi, E. Hazan, and Y. Singer, “Adaptive subgradient methods for online learning and stochastic optimization,” J. Mach. Learn. Res. **12**, 2121–2159 (2011).